Oxygen-Enhanced MR Imaging of Mice Lungs

K.N. Watt,[1,2] J. Bishop,[1] B.J. Nieman,[1,2] R.M. Henkelman,[1,2] and X.J. Chen[1,2]

Inhaled molecular oxygen has been widely used in humans to evaluate pulmonary ventilation using MRI. MR imaging has recently played a greater role in examining the morphologic and physiologic characteristics of mouse models of lung disease where structural changes are highly correlated to abnormalities in respiratory function. The motivation of this work is to develop oxygen-enhanced MR imaging for mice. Conventional human MR techniques cannot be directly applied to mouse imaging due to smaller dimensions and faster cardiac and respiratory physiology. This study examines the development of oxygen-enhanced MR as a noninvasive tool to assess regional ventilation in spontaneously breathing mice. An optimized cardiac-triggered, respiratory-gated fast spin-echo imaging sequence was developed to address demands of attaining adequate signal from the parenchyma, maintaining practical acquisition times, and compensating for rapid physiological motion. On average, a 20% T_1-shortening effect was observed in mice breathing 100% oxygen as compared to air. The effect of ventilation was shown as a significant signal intensity increase of 11% to 16% in the mouse parenchyma with 100% oxygen inhalation. This work demonstrates that adequate contrast and resolution can be achieved using oxygen-enhanced MR to visualize ventilation, providing an effective technique to study ventilation defects in mice. Magn Reson Med 59:1412–1421, 2008.

Key words: lung MRI; mouse; ventilation; oxygen-enhanced

Oxygen-enhanced MR imaging is a novel technique used to assess regional ventilation of the lung using inhaled molecular oxygen as a contrast agent (1). Molecular oxygen is weakly paramagnetic, and the effect of ventilation is visualized by signal intensity increase in MR images of the lung parenchyma acquired with subjects breathing 100% oxygen as compared to room air. During gas exchange, oxygen diffuses across the alveolar membrane and into the pulmonary capillary blood, coupling with hemoglobin to form oxyhemoglobin as well as dissolving into blood plasma as molecular oxygen (2). The latter contributes to a reduction in the longitudinal relaxation time of surrounding protons in the pulmonary blood that can be detected by T_1-weighted MR imaging as regions of increased signal intensity. The T_1-shortening effect is mainly attributed to the excess molecular oxygen because the concentration dissolved in the blood is raised by three- to fivefold with 100% oxygen inhalation, an increase much greater than for the amount of oxygen bound to hemoglobin when breathing 100% oxygen (2,3). Hence, oxygen-enhanced MR provides functional information about the combined ventilation, oxygen diffusion, and perfusion physiology of the lung.

Proton MR imaging of the lung, including oxygen-enhanced MR, is challenged by the unique morphology and physiology of the lung. The low proton density of the inflated lung tissue, multiple air-tissue interfaces of the alveoli, and movement of the chest all result in poor image quality due to reduced MR signal, large magnetic susceptibility gradients, and respiratory and cardiac motion artifacts in turn (4–6). To accommodate the low proton density and short apparent transverse relaxation time (T_2^*) of the air-filled parenchyma, a variety of short echo time (TE) imaging sequences have been designed to capture the available signal before it dephases (1,7,8) and, hence, to maximize contrast between images acquired with 100% oxygen and air inhalation (9). In addition, strategies such as breath-hold (10) and cardiac and respiratory gating techniques (11–13) have been applied to oxygen-enhanced imaging in humans to eliminate motion-related artifacts.

A growing interest in mouse models of pulmonary disease (14–17) drives the development of MR imaging for the study of anatomical and functional changes induced in the mouse lung. Application of oxygen-enhanced ventilation imaging in mice is also desirable but suffers from several difficulties in addition to and including those faced in human pulmonary MR. To obtain images with anatomical-definition comparable to human studies, mouse imaging demands a dramatic increase in spatial resolution because lung volumes are approximately 3000 times smaller (18). Imaging with significantly smaller voxel sizes results in a substantial decrease in signal-to-noise (SNR). This SNR decrease can in part be recovered by using higher field strengths, specialized RF coils and stronger gradients, and longer acquisition times for increased averaging. The gain at higher field strengths, however, may not be realized in lung imaging due to the presence of susceptibility artifacts.

The challenge of capturing the low signal from the parenchyma is further exacerbated by motion from cardiac and respiratory physiology. Motion-related artifacts cannot be eliminated in mouse imaging using the same methods that are prevalent in human imaging. Traditional breath-hold and quiet-breathing paradigms are clearly not possible in the mouse. In lung imaging, failure to properly gate for motion can introduce ghosting and partial volume blurring artifacts and places constraints on spatial resolution and imaging time in small animal imaging (19). Implementation of a successful gating strategy must consider several characteristics of mouse cardiac and respiratory physiology. First of all, mice have much faster heart and breathing rates than humans, which intensify motion artifacts and pose significant implications for cardiac and respiratory gating strategies (20). Second, natural fluctuations in cardiac and respiratory rate can produce artifacts

[1]Mouse Imaging Centre, Toronto Centre for Phenogenomics, Toronto, Ontario, Canada.

[2]Department of Medical Biophysics, University of Toronto, Ontario, Canada.

*Correspondence to: Kristina N. Watt, Mouse Imaging Centre, Hospital for Sick Children, Toronto Centre for Phenogenomics, 25 Orde Street, Toronto, Ontario, Canada M5T 3H7. E-mail: kwatt@sri.utoronto.ca.

Received 1 June 2007; revised 10 October 2007; accepted 24 November 2007.

DOI 10.1002/mrm.21517

Published online 17 April 2008 in Wiley InterScience (www.interscience.wiley.com).

when the length of the repetition periods (TR) vary based on gated acquisition. This occurs in conventional thoracic imaging that combines cardiac triggering and respiratory gating where data collection is intermittently halted (or blanked) to avoid acquisition during intervals of detectable respiratory motion, such as the gasp or breath-hold periods. Mechanical ventilation is often used to provide consistent breathing patterns for ventilation-synchronous pulmonary imaging in rodents (21,22), but this is far from natural physiological conditions. In addition, the procedure is invasive and technically challenging at the small-scale of the mouse lung.

Free-breathing proton MR imaging techniques have the potential to provide a more accurate and representative assessment of pulmonary function in small animals. The aim of the present work is to develop oxygen-enhanced MR imaging as a noninvasive tool to examine ventilation in spontaneously breathing mice. The main aspects of imaging considered in the development of this technique for mice are (i) the measurement of relaxation times in lung tissue to establish the timing constraints for pulse sequence optimization, (ii) the examination of oxygen-induced changes in T_1 relaxation time of the parenchyma to assess the signal intensity increases expected under the oxygen-enhanced protocol, and (iii) the evaluation of prospective motion gating strategies to compare cardiac-triggered schemes that use conventional respiratory blanking and respiratory gating with maintenance of steady-state magnetization. This study addresses the imaging challenges of low signal and motion artifacts specific to the size and physiology of the mouse and demonstrates the ability to visualize regional ventilation using an optimized cardiac-triggered, respiratory-gated three-dimensional (3D) fast spin-echo (FSE) sequence for oxygen-enhanced imaging.

METHODS

Twenty-one female C57/BL6 mice (Charles River Laboratories, Wilmington, MA) were used throughout the study (~21–25 g). All animal protocols were approved by the Hospital for Sick Children Animal Care Committee.

Fixed Lung Preparation

For preparation of the fixed lung specimen, the mouse was overdosed with a mixture of ketamine (Ketalean®, Bimeda-MTC, Cambridge, Ontario, Canada) and xylazine (Rompun®, Bayer Inc., Toronto, Ontario, Canada) administered intraperitoneally. Immediately after sacrifice, the trachea of the mouse was ligated with a silk suture and the inflated whole lung was excised from the animal and fixed in 10% buffered formalin phosphate (Fisher Scientific Inc., Fairlawn, NJ). Before in vitro relaxometry, the sample was rinsed and immersed in fluorinert (3M Specialty Materials Markets Group, Harmeslaan, Belgium) within a tightly sealed plastic tube (diameter = 13 mm, length = 40 mm) at room temperature (20–22°C).

Fixed Animal Preparation

The whole-body fixed mouse with partially inflated lungs was prepared using a high-frequency ultrasound-guided protocol similar to that previously outlined by Zhou et al. (23). The mouse was perfused in the closed-chested procedure with a solution of heparin and saline followed by 10% buffered formalin phosphate, without administration of any contrast agent. To ensure that the lungs remained inflated, a 24-gauge intravenous catheter was introduced into the trachea early in the perfusion procedure and approximately 0.3 mL to 0.5 mL of air was slowly injected into the lung. The trachea was then ligated with a silk suture and the incision was sealed with adhesive (Vetbond® Tissue Adhesive, 3M Animal Care Products, St. Paul, MN).

Live Animal Preparation

Mouse handling for the imaging studies were performed as follows. Mice were anesthetized in an induction chamber with 4.0% vaporized isoflurane (Baxter Corp., Toronto, ON, Canada) in 100% oxygen before imaging. In the prone position, the mouse was loaded on a custom built sled (24) outfitted with a set of electrocardiograph (ECG) leads fastened to the shaved chest, a pneumatic pillow positioned under the abdomen, and a thermocouple skin probe. These transducers provided real-time monitoring of ECG, respiratory events, and body temperature (Small Animal Instruments Inc., Stoneybrook, NY). Mice were anesthetized with 1.4% to 1.6% isoflurane administered through a nose cone during imaging, alternating between 100% oxygen and room air at 1.2 L/min depending on the scan of interest in the oxygen-enhanced imaging protocol. The gas flow surrounding each mouse was warmed to maintain a skin temperature of ~32°C over the course of imaging. All measurements were performed on spontaneously breathing animals.

MR Relaxation Measurements

To assess the relaxation properties of lung tissue for optimizing the live imaging pulse sequence, measurements of T_1, T_2, and T_2^* relaxation times at 7 Tesla (T) were made of an excised, inflated, fixed lung specimen. Whole organ MR relaxometry was performed on the sample with a 7T MRI scanner (Varian INOVA, Palo Alto, CA) and a 6-cm inner diameter insert gradient coil (Magnex 115/60) with 1000-mT/m maximum amplitude and 150-μs rise time. The T_1, T_2, and T_2^* relaxation times of the specimen immersed in fluorinert were measured using inversion recovery (IR), Carr-Purcell-Meiboom-Gill (CPMG), and 90°-pulse sequences, respectively. For the measurement of T_1, the inversion time (TI) was varied from 5 ms to 5905 ms and total of 60 points was acquired in 22 min. For the measurement of T_2, the interpulse delay time for the CPMG was 2 ms and 20 points were obtained in 25 min. A 4-s delay allowed for longitudinal recovery between individual measurements during the T_1 and T_2 experiments. The acquisition time for the measurement of T_2^* was 10 ms. A three-parameter nonlinear least squares method was used to fit the data to exponential recovery $[1 - 2\exp(-TI/T_1)]$ and to exponential decay $[\exp(-TE/T_2)]$, and $[\exp(-TE/T_2^*)]$ from which T_1, T_2, and T_2^* values were derived, respectively. Data analysis was performed with standard MATLAB software (v 6.5.0 release 13, The MathWorks, Inc., Natick, MA).

T_1 Measurements With Oxygen-enhancement

To examine changes in T_1 relaxation due to 100% oxygen gas inhalation, in vivo T_1 measurements of lung tissue were conducted on two mice. Each mouse was imaged over two sessions where the mouse breathed 100% oxygen or room air. Nine images were acquired in each session using an inversion recovery 3D FSE sequence in which TI was varied from 200 ms to 1800 ms. Respiratory gating (with blanking during the breath-hold period) restricted data acquisition to the end-expiration period of the breathing cycle to reduce motion artifacts. TR was based on the length of the end-expiration period and varied typically between 2300 ms and 2700 ms. Images were acquired with effective echo time TE_{eff} = 2 ms, echo train length ETL = 8, echo spacing ESP = 2 ms, two averages, field of view (FOV) 60 × 30 × 20 mm, and matrix size 256 × 128 × 12 for a scan time of approximately 17 min per image. Image reconstruction and analysis was performed using MATLAB. From each 3D image data set, a 2D coronal slice was selected at a similar position dorsal from the heart and away from large airways and vessels. Average signal intensities were determined for regions-of-interest (ROIs) located in the parenchyma of the right and left lobes. T_1 values were derived by curve fitting the signal intensities using a three-parameter nonlinear least squares method based on exponential recovery $[1 - 2\exp(-TI/T_1)]$.

Evaluation of Motion Gating Strategies

Oxygen-enhanced MR imaging is particularly sensitive to motion artifact because ventilation is visualized based on the difference between images of the parenchyma acquired with 100% oxygen and air inhalation that have inherently low SNR. The impact of cardiac and respiratory motion can be suppressed using conventional gating techniques that use combined cardiac-triggered and respiratory-blanked schemes. In such schemes, however, data acquisition occurs at irregular intervals based on fluctuations in cardiac and respiratory rates. As a result, steady-state longitudinal magnetization is not preserved and artifacts can be introduced as signal intensity variations in the image. This study aimed to investigate and minimize unwanted artifacts associated with conventional motion gating strategies for lung imaging. It compares the performance of different cardiac-triggered schemes that apply conventional respiratory blanking and respiratory gating with the maintenance of steady-state magnetization in addressing the natural variations in cardiac and respiratory rates without confounding changes in signal intensity.

An experiment examining the effects of imaging with constant versus variable TR was conducted on a fixed mouse in the scanner and with a live anesthetized mouse (25 g) maintained outside of the scanner providing the physiological timing control signals. Performance of the different acquisition schemes were evaluated on a fixed mouse to avoid confounding artifacts from physiological motion. First, a reference data set was acquired with a constant TR of 300 ms and total imaging time of ~21 min (Scheme A, Fig. 1). A second data set was acquired with a conventional cardiac-triggered, respiratory-blanked (during gasp periods) scheme (Scheme B, Fig. 1). A variable TR of two cardiac R-R intervals was used (on average 310 ms based on the real-time monitoring of the anesthetized mouse), and the total imaging time was ~28 min. The final data set was acquired with a cardiac-triggered, respiratory-gated scheme with dummy scans to maintain steady-state magnetization (Scheme C, Fig. 1). Data collection only occurred during the acquisition scans and four echo trains were obtained every end-expiration period. A variable TR of two cardiac R-R intervals was used (on average 280 ms) and the total imaging time was ~65 min. Aside from differences in TR, all data sets were acquired with the 3D FSE sequence using common parameters TE_{eff} = 2 ms, ETL = 8, ESP = 2 ms, two averages, FOV 60 × 30 × 30 mm, and matrix size 256 × 128 × 128.

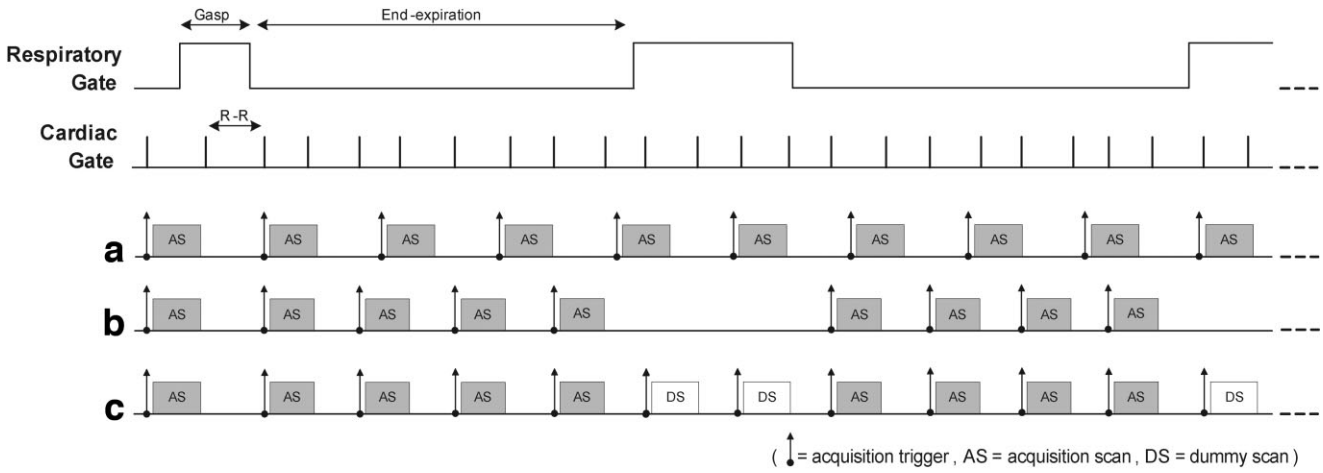

FIG. 1. Diagram of the physiological events and constant and variable TR gating schemes used in the evaluation of different motion gating strategies. The respiratory and cardiac gates (top) were obtained from the real-time monitoring of an anesthetized mouse maintained outside the scanner. Image acquisition was performed on a fixed mouse with the following schemes (bottom): (**A**) Constant TR, (**B**) cardiac-triggered, respiratory-blanked (during the gasp periods), and (**C**) cardiac-triggered, respiratory-gated (with dummy scans).

Oxygen-Enhanced Imaging

An oxygen-enhanced ventilation imaging study was conducted on five mice. Imaging was performed with a 3D FSE sequence using a cardiac-triggered, respiratory-gated scheme with dummy scans for maintenance of steady-state magnetization. Four echo trains were obtained every end-expiration period. A constant ECG trigger delay was used to help restrict data acquisition to the diastolic phase of the cardiac cycle. During diastole, the signal from the parenchyma increases, because blood flow is slower and less turbulent than in systole (25). An image resolution of 234 μm-isotropic was obtained using the parameters TE_{eff} = 2 ms, ETL = 8, ESP = 2 ms, two averages, FOV 60 × 30 × 30 mm, and matrix size 256 × 128 × 128. A TR of two cardiac R-R intervals (R-R ~ 270–286 ms) was used to attain greater signal from the lung parenchyma. Scan time for each image was approximately 55 to 75 min. Four sets of images were acquired for each mouse in interleaved sessions, two with 100% oxygen inhalation and two with air inhalation. A 5- to 10-min delay separated each scan to allow for switching and equilibrating between gases. Average 100% oxygen and air images were formed in postprocessing (four averages total). From each of these 3D data sets, three consecutive 2D coronal slices were selected at a similar position dorsal from the heart to avoid contributions from the major vessels. Average signal intensities were measured in ROIs consisting of the right and left lung lobes. Percent signal enhancement was determined by dividing the average signal intensity of the 100% oxygen ROI by that of the air ROI. Based on the averaged images, lung ventilation was depicted in relative enhancement maps that expressed each pixel as a percent change in signal intensity (SI) as described by Edelman et al. (1), $[(SI_{100\%\,Oxygen}) - (SI_{Air})]/SI_{Air}$, where $SI_{100\%\ Oxygen}$ and SI_{Air} are the signal intensity of the parenchyma with 100% oxygen and air inhalation, respectively.

RESULTS

MR Relaxation Measurements

The longitudinal and transverse relaxation times T_1, T_2, and T_2^* of the excised inflated lung specimen were measured to be T_1 = 1256 ± 17 ms, T_2 = 44.8 ± 9.5 ms, and T_2^* = 2.1 ± 0.8 ms, respectively. As expected, the inhomogeneous nature of the alveolar tissue contributes to rapid signal loss and results in a very short value for T_2^*. It is likely that this value is much shorter for in vivo imaging due to changes in tissue inflation and heterogeneity over the respiratory cycle, particularly during inspiration. This is consistent with studies performed in spontaneously breathing rats and mice that have reported T_2^* values between 400 μs and 600 μs at 4.7T (26).

T_1 Measurements With Oxygen-enhancement

The examination of longitudinal relaxation times under the oxygen-enhanced protocol yielded T_1 values comparable to that measured in vitro. With inhalation of 100% oxygen, the mean T_1 relaxation times were 1140 ± 209 ms and 1087 ± 16 ms in the right and left lung lobes, respectively. With inhalation of room air, T_1 relaxation times were 1397 ± 28 ms and 1385 ± 194 ms in the right and left lungs, respectively. On average, T_1 values in the right and left lobes were reduced by 18% ± 13% and 21% ± 10% respectively, when breathing 100% oxygen as compared with air.

Evaluation of Motion Gating Strategies

Figure 2 demonstrates the ghosting artifacts introduced when variations in cardiac and respiratory rates modulate recovery of the longitudinal magnetization of the MR signal. With the conventional Scheme B (cardiac-triggered, respiratory-blanked), the imaging sequence is halted during the respiratory gasp periods that frequently fluctuate in length due to natural variation or inaccurate detection of the mouse breathing patterns by the pneumatic pillow and/or monitoring software. Using this gating approach, the high variation in the TR of the acquisition scans result in ghosts that contribute to an increase in background noise of 48% (Fig. 2B) relative to the benchmark image acquired with Scheme A (Fig. 1A). Likewise, the SNR of the lung tissue is reduced by 39% relative to the benchmark image as shown in Table 1_1. Background noise is measured as the standard deviation of the signal intensity magnitude of a ROI located in the air background of the image (Fig. 2, top). With the implementation of dummy scans during the gasp periods (Scheme C), however, only a 5% increase in background noise of the acquired image (Fig. 2C) is detected relative to the benchmark image. The dummy scans maintained the steady-state longitudinal magnetization by continued RF excitation of spins without collection of image data during the gasp periods. Table 1 shows a 20% decrease in lung SNR of the Scheme C image relative to the benchmark image but this can be attributed to lower lung signal intensity likely arising from the shorter TR periods rather than an increase in background noise. The extent of the ghosting artifacts is revealed in difference images (Fig. 2, bottom) where the constant TR image is subtracted from images acquired with Scheme B and Scheme C. Although some ghosting artifacts are still introduced when variations in cardiac rate (Fig. 2B,C) modulate recovery of the longitudinal magnetization, the artifacts to a larger extent are attributed to fluctuations in respiratory rate. This finding is evident in the substantial reduction in ghosts observed in the image acquired with Scheme C (Fig. 2C) compared to that obtained with Scheme B. This reduction is attributed to the use of dummy scans in Scheme C to eliminate the effects due to variations in respiratory rate. Hence, a gating strategy based on Scheme C, which maintains steady-state magnetization, was chosen for the free-breathing oxygen-enhanced imaging protocol.

Oxygen-enhanced Imaging

Figure 3 shows T_1-weighted oxygen-enhanced images of a mouse spontaneously breathing 100% oxygen and air and the corresponding relative enhancement maps. To aid visualization, the data obtained from the 3D acquisitions are shown as 2D images at similar slice positions. Examination of the coronal images acquired under the oxygen-enhanced protocol reveals a relative signal intensity increase with pure oxygen inhalation of 30% and 21% in the right and left lobes, respectively. The relative enhancement map of the images shows similar signal enhancement

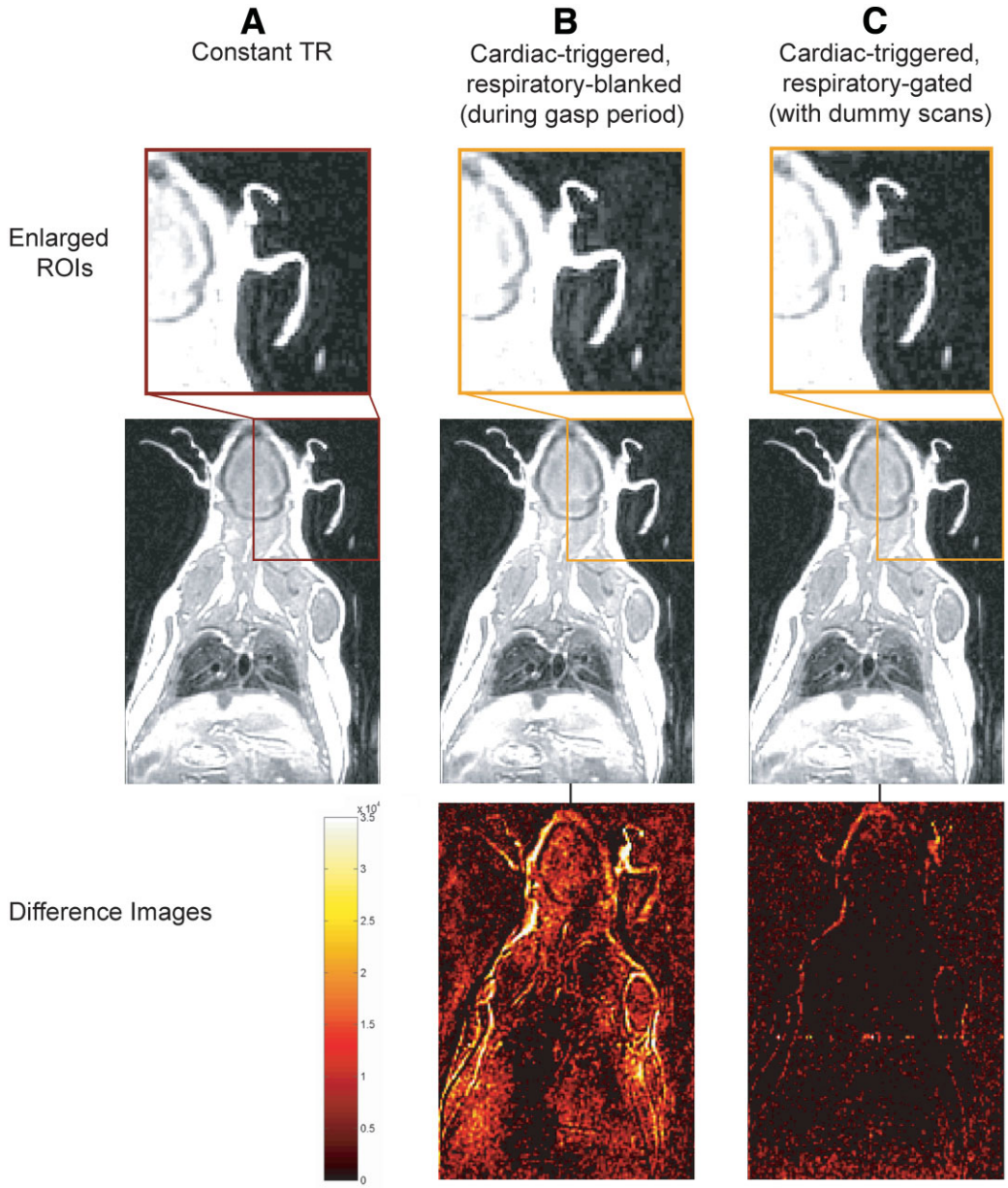

FIG. 2. Coronal three-dimensional (3D) fast spin-echo (FSE) images of a fixed mouse (24 g) obtained with different acquisition schemes: (**A**) Constant TR and (**B,C**) variable TR based on the real-time monitoring of an anesthetized mouse maintained outside the scanner. Enlarged regions-of-interest (ROIs, top) from original images (middle) reveal differences in background noise introduced by ghosting artifacts. Difference images (bottom) were formed by the subtraction of the constant TR image (A) from the cardiac-triggered, respiratory-blanked image (B) and the cardiac-triggered, respiratory-gated image (C). All images within rows are scaled to the same intensity.

in the parenchyma with pure oxygen inhalation and greater increases (~60–70%) are observed in regions surrounding the larger pulmonary vessels. As evident in Figure 4, signal enhancement in the lung is also greater than enhancement detected in the surrounding body tissue with pure oxygen inhalation which is only 5% to 10%.

Figure 5 shows the relative change in signal intensity of the lung parenchyma with 100% oxygen inhalation ob-

Table 1
Comparison of Signal-to-Noise (SNR) of Images Acquired With Constant and Variable TR Acquisition Schemes

Image acquired with scheme	Background noise and artifact (a.u. intensity × 10^3)	Lung signal (a.u. intensity × 10^3)	$SNR_{lung/background}$
A-Constant TR	2.1	32.9	15.7
B-Respiratory-blanked	3.1	29.6	9.5
C-Respiratory-gated (with dummy scans)	2.2	27.4	12.5

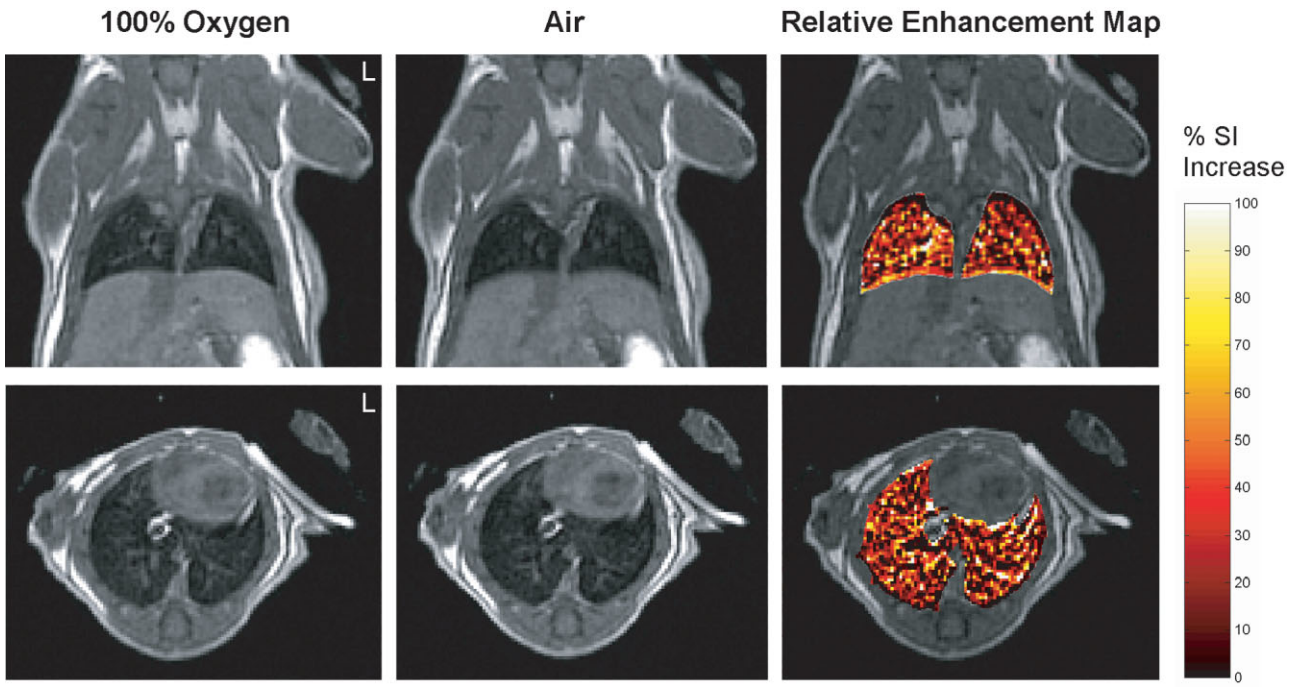

FIG. 3. Oxygen-enhanced images of a normal mouse breathing 100% oxygen and air. Coronal (top) and axial (bottom) images were acquired using a three-dimensional (3D) fast spin-echo (FSE) cardiac-triggered, respiratory-gated sequence with dummy scans. The relative enhancement map shows the percent increase of signal intensity in the lungs observed with 100% oxygen inhalation relative to air for images at the same slice position. To highlight signal enhancement in the lung, the intensity changes in the rest of the body have been masked. All coronal images are shown at a position dorsal from the heart and away from major vessels.

served for all five mice examined. Relative to the images acquired breathing air, an average signal intensity increase of 16% ± 9% and 11% ± 7% (mean ± standard deviation) was detected in the right and left lobes, respectively. These signal intensity changes with oxygen enhancement were considered significant for $P < 0.05$ by the paired Student *t*-test. Although enhancement was slightly greater in right lobes than in the left lobes, these findings were not at a level of significance. The SNR per voxel over the lung lobes was approximately 20 ± 3 and 18 ± 2 for the five mice breathing 100% oxygen and air, respectively.

DISCUSSION

To our knowledge, this work demonstrates the first application of oxygen-enhanced MR imaging to the study of ventilation in spontaneously breathing mice. Visualization of signal intensity changes in the lung parenchyma under the oxygen-enhanced protocol was achieved by implementing a 3D FSE sequence with both short echo spacing and TR in combination with a cardiac-triggered, respiratory-gated acquisition to help overcome the challenges faced in pulmonary MR imaging of mice. Previous proton MRI studies have shown the effectiveness of 2D gradient echo sequences (26,27) and more recently spin echo sequences (28,29) in detecting anatomical abnormalities, tumors, and respiratory diseases in mice lungs. The evaluation of lung function using free-breathing proton MR imaging has only been recently explored in rats with similar findings using gradient echo sequences based on T_2^* weighting (30,31).

This study demonstrates the feasibility of using a 3D FSE sequence for the assessment of lung ventilation. The oxygen-enhanced MR technique provides functional information about respiration physiology, where the diffusion of oxygen from the alveolar airspaces into the pulmonary vasculature is depicted as regions of increased signal intensity on images. Unlike the imaging of hyperpolarized noble gases (32), oxygen-enhanced MR does not examine the gas directly but visualizes the regional effect of oxygen after transfer into the pulmonary vasculature. Thus, the present technique can offer valuable information about combined ventilation, diffusion, and perfusion in the lung. The performance of oxygen-enhanced MR relies heavily on the ability to image the parenchyma because ventilation is observed as a signal difference in the tissue between 100% oxygen and air inhalation. It is well known that signal in the lung is weak due to the low proton density and variations in susceptibility arising from the multiple air-tissue interfaces of the alveoli. The latter effect is reflected in the short value of T_2^* measured (~2 ms). The work presented here takes advantage of the moderate value of T_2 value (~45 ms) to provide greater signal from the parenchyma by using a 3D FSE sequence. The multi-echo implementation with short echo spacing is also less sensitive to tissue magnetic susceptibility variations and diffusion effects compared to conventional single echo acquisitions. It provides a fast rate of data acquisition where scan time efficiency is mainly reduced by the prolonged repetition periods required to ensure sufficient recovery given the lengthy T_1 relaxation time measured (~1256 ms) at high field. The transverse and longitudinal relaxation

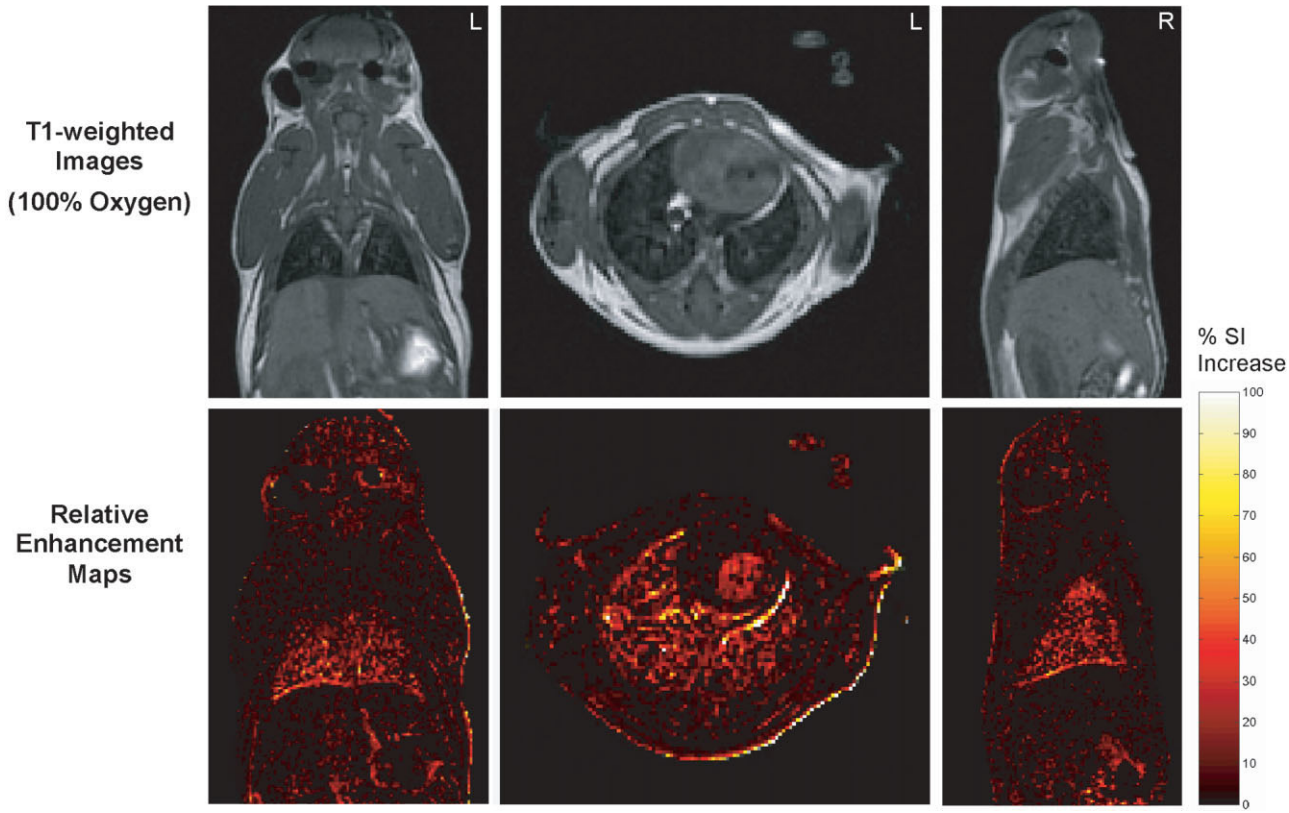

FIG. 4. Relative enhancement maps of a normal mouse (23 g) shown in different orientations. Coronal (left), axial (middle), and sagittal (right) enhancement maps formed from images acquired with the oxygen-enhanced protocol using the three-dimensional (3D) fast spin-echo (FSE) cardiac-triggered, respiratory-gated sequence. Signal enhancement is higher in the lung parenchyma of the lung and left heart ventricle relative to other tissues in the body. To highlight signal enhancement in the mouse, the signal outside of the body has been masked. T_1-weighted images (top) provide an anatomical reference for the maps. Coronal and sagittal images are shown at a position dorsal from the heart and away from major vessels with the sagittal slices centered through the right lung lobes.

times measured in this study follow trends in the existing literature of similar in vitro studies performed in rats and mice (33–36) and provided direction for the selection of sequence parameters for live imaging.

Investigating conventional prospectively triggered and gated techniques at high field is critical because motion artifacts arising from breathing are more pronounced at these field strengths (37). This study revealed that ghosting artifacts are introduced in conventional cardiac-triggered, respiratory-blanked gating schemes and are mainly attributed to T_1 effects from variable respiratory rates rather than cardiac rates (Fig. 2). The intensity of the artifacts is reduced by 43% with the application of dummy scans during periods with no acquisition, which maintain more constant excitation throughout the entire acquisition (Table 1). Similar findings have been reported for imaging of cardiac anatomy in mice at high field (20). A gating strategy that preserves a consistent spin environment throughout image acquisition is necessary to improve the sensitivity of oxygen-enhanced MR, because the subtraction technique is based on the detection of subtle signal intensity differences for the evaluation of ventilation defects.

A limitation of the cardiac-triggered, respiratory-gated scheme with dummy scans is its prolonged imaging time over conventional and non-gated approaches. In the current fixed mouse study, scan time doubled with cardiac-

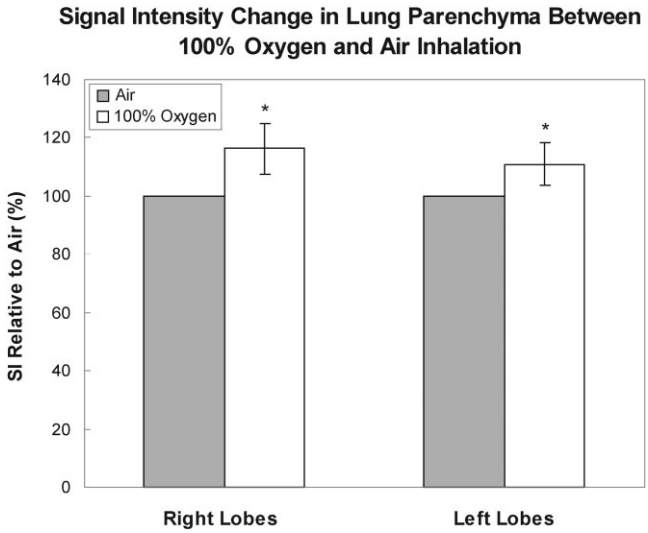

FIG. 5. Percent change in signal intensity of the parenchyma for normal mice with the oxygen-enhanced protocol (mean ± standard deviation, n = 5). A 16% and 11% signal intensity increase with pure oxygen inhalation was observed in the right and left lobes respectively. Measurements were performed at a similar slice position in each mouse (representative coronal slices shown in Fig. 3). Significant findings are reported at the $P < 0.05$ level (*) based on a paired Student *t*-test.

triggered, respiratory-gated imaging using dummy scans (Scheme C) over conventional imaging (Scheme B), because the number of acquisition scans (echo trains) executed per end-expiration period was predefined by the user in Scheme C. Limiting the number of acquisition scans based on observing mouse physiology before acquisition ensured that all data were collected well within the end-expiration periods with the least possible corruption by motion from subsequent inspirations. Retrospective cardiac and respiratory gating (38) was also considered as an alternative strategy for suppressing motion artifacts, particularly for the future application of the oxygen-enhanced technique to compromised mice that exhibit erratic breathing behavior. While steady-state longitudinal magnetization is preserved with retrospective techniques, the relatively long TR of the imaging sequence (on average 300 ms) remains the limiting factor for attaining higher scan efficiency while obtaining adequate SNR from the parenchyma. As shown in mouse brain imaging at high field (39), it is possible to use partial excitation FSE to reduce the TR while conserving longitudinal magnetization, but additional scan time is still required for oversampling to compensate for loss of data discarded in the sorting and image reconstruction process. It is estimated that at least four to five times oversampling of *k*-space would be needed to form a single image data set, which places tight constraints on scan time because the oxygen-enhanced imaging protocol involves the acquisition of multiple images with 100% oxygen and air inhalation within an imaging session.

The significant increase in signal intensity observed in the mouse parenchyma with 100% oxygen inhalation demonstrates that sufficient contrast can be attained using oxygen-enhanced MR to visualize the effect of ventilation. The T_1 values measured in mice under the oxygen-enhanced protocol reveal an average reduction of T_1 by 20%, which is comparable to findings of oxygen-enhanced MR human studies that have reported T_1-shortening between 9% and 17% (1,10,40). The T_1 measurements indicate that a signal enhancement of 20% and 24% could be expected due to the T_1-shortening effect of molecular oxygen in the right and left lobes, respectively. The results for the five mice in this study are slightly lower, averaging 16% and 11% for the right and left lobes, with a 7% to 8% standard deviation (Fig. 5). These values are detected in the bulk parenchyma of the lung, which exhibits relatively homogeneous enhancement (Figs. 3, 4). The enhancement pattern is likely attributed to the normal diffusion of oxygen from the alveolar airspace into the blood capillaries. Further examination of mouse models with abnormal ventilation will help to determine the degree to which this mechanism contributes to the signal enhancement. As expected, relative enhancement maps reveal that signal enhancement with pure oxygen inhalation was greater in the lung parenchyma than in surrounding tissue such as the liver, skeletal muscle, and subcutaneous fat. This finding is highlighted in Figure 4 and is in agreement with previous findings in humans that reported no significant oxygen-induced T_1-shortening in the surrounding tissues but observed the effect in the arterial blood of the left heart ventricle and lung parenchyma (1,2). The greater enhancement localized in the lungs of the mice further indicates that the signal intensity increases observed reflect oxygen absorption and ventilation in the parenchyma due to oxygen-induced T_1-shortening of pulmonary blood.

Variations in signal enhancement of the lung for a given subject can be attributed to factors associated with image acquisition. Small regions of high signal enhancement that border the edges of the lung lobes or nearby structures, such as the heart and inferior vena cava, are likely a result of motion. Although the monitoring sled ensured minimal postural changes in a subject during an imaging session, high intensity artifacts can arise in the enhancement maps when the interfaces between surrounding tissues and air in the lung shift during the successive acquisition of 100% oxygen and air images. Enhancement maps of several mice reveal that edge artifacts primarily appear as a thin band of high enhancement bordering the diaphragm (Figs. 3, 4, coronal and sagittal images) and lining the outer myocardium of the heart adjacent to the lung airspace (Figs. 3, 4, axial images). As anticipated, the consistency and location of the artifacts indicate that the diaphragm and myocardium are structures most affected by motion from breathing and cardiac activity. Image registration techniques (41) that spatially align successive images acquired with the oxygen-enhanced protocol may prove effective in reducing such motion-related artifacts in the future.

Variability in signal enhancement observed between subjects breathing 100% oxygen and air can be related to image analysis and natural physiology. Variability in measurements may arise from the manual selection of lung ROIs, which consisted of the entire right or left lobes. The presence of small vessels and airways in these regions can contribute slight differences in signal enhancement measured between mice. Variations in pulmonary structure or blood flow may account for the differences in enhancement observed between the right and left lobes as oxygen-enhanced studies in humans have also revealed that T_1 values are not homogeneous across the entire lung (10). Gating successfully confines data acquisition to end-expiration but it is still difficult to ensure that imaging occurs at a consistent lung volume for all mice studied. Signal intensity of the parenchyma can be affected by changes in inflation state (42) as well as cardiac blood flow effects (25). The application of the ECG trigger delay during imaging helped to minimize temporal blood flow effects in this study by restricting data acquisition to diastole.

The examination of individual T_1-weighted images acquired breathing 100% oxygen or air (Figs. 3, 4) show no artifacts in the thorax arising from motion of the diaphragm and heart, even along the phase-encode (dorsal–ventral and right–left lateral) directions. At the resolution used, the images provide sufficient anatomical detail to delineate between the edges of the lung and surrounding tissue as well as to detect the parenchyma, large airways, and cardiac and pulmonary vessels within the lung. The absence of ghosts attests to the robustness of the 3D cardiac-triggered, respiratory-gated scanning strategy in suppressing artifacts arising from physiological motion and conventionally gated acquisitions schemes in free-breathing mice. This conclusion is in line with previous work using combined 2D cardiac-triggered, respiratory-gated acquisition schemes, which have been shown to be superior to their individual counterparts for motion control in car-

diac mouse imaging (20), thoracic rat imaging (19), and oxygen-enhanced human lung imaging (9). Limiting data acquisition to the quiescent periods of the cardiac and respiratory cycles through triggering and gating effectively reduced the intensity of image ghosts. The application of anesthetic over the long imaging session also resulted in slower respiratory rates (~25 to 35 breaths/min), further decreasing the amplitude and frequency of motion from the diaphragm. The 3D images reveal the benefit of averaging along a second phase-encode direction, which helps to attenuate systematic ghosts and random noise and provide increased coverage of the entire lung.

CONCLUSIONS

This work demonstrates the first application of oxygen-enhanced MR imaging to the study of ventilation in spontaneously breathing mice. A cardiac-triggered, respiratory-gated 3D fast spin-echo sequence has been shown to provide high quality and virtually artifact-free images of the lung parenchyma under the oxygen-enhanced protocol. The sequence is capable of gathering image data at similar positions in the cardiac and respiratory cycle and the combined gating scheme that uses the maintenance of steady-state magnetization is required to limit artifacts generated from variable recovery between cardiac and respiratory events. Using this sequence and acquisition scheme, the effect of ventilation can be non-invasively visualized as a significant signal intensity increase in the parenchyma with 100% oxygen inhalation. The results show the ability to overcome the unique challenges of pulmonary MR in mice, and the technique offers the foundation upon which oxygen-enhanced MR can be used to investigate abnormal lung function in mouse models of respiratory disease.

ACKNOWLEDGMENTS

The authors thank Lori Davidson and Jun Dazai for technical assistance with animal experiments and Akiva Feintuch for helpful discussion and advice.

REFERENCES

1. Edelman RR, Hatabu H, Tadamura E, Li W, Prasad PV. Noninvasive assessment of regional ventilation in the human lung using oxygen-enhanced magnetic resonance imaging. Nat Med 1996;2:1236–1239.
2. Tadamura E, Hatabu H, Li W, Prasad PV. Edelman RR. Effect of oxygen inhalation on relaxation times in various tissues. J Magn Reson Imaging 1997;7:220–225.
3. Silvennoinen MJ, Kettunen MI, Kauppinen RA. Effects of hematocrit and oxygen saturation level on blood spin-lattice relaxation. Magn Reson Med 2003;49:568–571.
4. Albertine KH. Structural organization and quantitative morphology of the lung. In: Cuttilo AG, editor. Application of magnetic resonance imaging to the study of lung. Armonk, NY: Futura Publishing; 1996. p 73–114.
5. Hatabu H, Alsop DC, Listerud J, Bonnet M, Gefter WB. T_2^* and proton density measurement of normal human lung parenchyma using submillisecond echo time gradient echo magnetic resonance imaging. Eur J Radiol 1999;29:245–252.
6. Bergin CJ, Glover GH, Pauly JM. Lung parenchyma: magnetic susceptibility in MR imaging. Radiology 1991;180:845–848.
7. Ohno Y, Hatabu H, Higashino T, Kawamitsu H, Watanabe H, Takenaka D, van Cauteren M, Sugimura K. Centrically reordered inversion recovery half-Fourier single-shot turbo spin-echo sequence: improvement of the image quality of oxygen-enhanced MRI. Eur J Radiol 2004;52:200–205.
8. Arnold JF, Fidler F, Wang T, Pracht ED, Schmidt M, Jakob PM. Imaging lung function using rapid dynamic acquisition of T_1-maps during oxygen enhancement. MAGMA 2004;16:246–253.
9. Mai VM, Chen Q, Bankier AA, Edelman RR. Multiple inversion recovery MR subtraction imaging of human ventilation from inhalation of room air and pure oxygen. Magn Reson Med 2000;43:913–916.
10. Loffler R, Muller CJ, Peller M, Penzkofer H, Deimling M, Schwaiblmair M, Scheidler J, Reiser M. Optimization and evaluation of the signal intensity change in multisection oxygen-enhanced MR lung imaging. Magn Reson Med 2000;43:860–866.
11. Vaninbroukx J, Bosmans H, Sunaert S, Demedts M, Delcroix M, Marchal G, Verschakelen J. The use of ECG and respiratory triggering to improve the sensitivity of oxygen-enhanced proton MRI of lung ventilation. Eur Radiol 2003;13:1260–1265.
12. Molinari F, Eichinger M, Fink C, Risse F, Bonomo L, Kauczor HU. Navigator-triggered oxygen-enhanced MRI in patients with interstitial lung disease. Proc Intl Soc Magn Reson Med 2006;14:35.
13. Molinari F, Gaudino S, Fink C, Corbo GM, Valente S, Pirronti T, Bonomo L. Simultaneous cardiac and respiratory synchronization in oxygen-enhanced magnetic resonance imaging of the lung using a pneumotachograph for respiratory monitoring. Invest Radiol 2006;41:476–485.
14. De Sanctis GT, Drazen JM. Genetics of native airway responsiveness in mice. Am J Respir Crit Care Med 1997;156:S82–S88.
15. Groneberg DA, Chung KF. Models of chronic obstructive pulmonary disease. Respir Res 2004;5:18.
16. D'Armiento J, Dalal SS, Okada Y, Berg RA, Chada K. Collagenase expression in the lungs of transgenic mice causes pulmonary emphysema. Cell 1992;71:955–961.
17. Mall M, Grubb BR, Harkema JR, O'Neal WK, Boucher RC. Increased airway epithelial Na+ absorption produces cystic fibrosis-like lung disease in mice. Nat Med 2004;10:487–493.
18. Braun A, Ernst H, Hoymann HG, Rittinghausen S. Respiratory tract. In: Hedrich H, editor. The handbook of experimental animals: the laboratory mouse. San Diego: Elsevier Academic Press; 2004. p 225–243.
19. Mai W, Badea CT, Wheeler CT, Hedlund LW, Johnson GA. Effects of breathing and cardiac motion on spatial resolution in the microscopic imaging of rodents. Magn Reson Med 2005;53:858–865.
20. Cassidy PJ, Schneider JE, Grieve SM, Lygate C, Neubauer S, Clarke K. Assessment of motion gating strategies for mouse magnetic resonance at high magnetic fields. J Magn Reson Imaging 2004;19:229–237.
21. Hedlund LW, Cofer GP, Owen SJ, Allan Johnson G. MR-compatible ventilator for small animals: computer-controlled ventilation for proton and noble gas imaging. Magn Reson Imaging 2000;18:753–759.
22. Chen BT, Yordanov AT, Johnson GA. Ventilation-synchronous magnetic resonance microscopy of pulmonary structure and ventilation in mice. Magn Reson Med 2005;53:69–75.
23. Zhou YQ, Davidson L, Henkelman RM, Nieman BJ, Foster FS, Yu LX, Chen XJ. Ultrasound-guided left-ventricular catheterization: a novel method of whole mouse perfusion for microimaging. Lab Invest 2004;84:385–389.
24. Dazai J, Bock NA, Nieman BJ, Davidson LM, Henkelman RM, Chen XJ. Multiple mouse biological loading and monitoring system for MRI. Magn Reson Med 2004;52:709–715.
25. Knight-Scott J, Keilholz-George SD, Mai VM, Christopher JM. Temporal dynamics of blood flow effects in half-Fourier fast spin echo ^{1}H magnetic resonance imaging of the human lungs. J Magn Reson Imaging 2001;14:411–418.
26. Beckmann N, Tigani B, Mazzoni L, Fozard JR. MRI of lung parenchyma in rats and mice using a gradient-echo sequence. NMR Biomed 2001;14:297–306.
27. Marzola P, Lanzoni A, Nicolato E, Di Modugno V, Cristofori P, Osculati F, Sbarbati A. ^{1}H MRI of pneumococcal pneumonia in a murine model. J Magn Reson Imaging 2005;22:170–174.
28. Garbow JR, Zhang Z, You M. Detection of primary lung tumors in rodents by magnetic resonance imaging. Cancer Res 2004;64:2740–2742.
29. Kubo S, Levantini E, Kobayashi S, Kocher O, Halmos B, Tenen DG, Takahashi M. Three-dimensional magnetic resonance microscopy of pulmonary solitary tumors in transgenic mice. Magn Reson Med 2006;56:698–703.

30. Beckmann N, Cannet C, Zurbruegg S, Rudin M, Tigani B. Proton MRI of lung parenchyma reflects allergen-induced airway remodeling and endotoxin-aroused hyporesponsiveness: a step toward ventilation studies in spontaneously breathing rats. Magn Reson Med 2004; 52:258–268.
31. Quintana HK, Cannet C, Zurbruegg S, Ble FX, Fozard JR, Page CP, Beckmann N. Proton MRI as a noninvasive tool to assess elastase-induced lung damage in spontaneously breathing rats. Magn Reson Med 2006;56:1242–1250.
32. Moller HE, Chen XJ, Saam B, Hagspiel KD, Johnson GA, Altes TA, de Lange EE, Kauczor HU. MRI of the lungs using hyperpolarized noble gases. Magn Reson Med 2002;47:1029–1051.
33. Shioya S, Haida M, Fukuzaki M. Characterization of experimental lung injury and clinical pulmonary disease by NMR relaxation measurements. In: Cuttilo AG, editor. Application of magnetic resonance imaging to the study of lung. Armonk, NY: Futura Publishing; 1996. p 227–286.
34. Kveder M, Zupancic I, Lahajnar G, Blinc R, Suput D, Ailion DC. Ganesan K. Goodrich C. Water proton NMR relaxation mechanisms in lung tissue. Magn Reson Med 1988;7:432–441.
35. Bottomley PA, Foster TH, Argersinger RE, Pfeifer LM. A review of normal tissue hydrogen NMR relaxation times and relaxation mechanisms from 1-100 MHz: dependence on tissue type. NMR frequency. temperature. species. excision. and age. Med Phys 1984;11:425–448.
36. Uematsu H, Wehrli SL, Takahashi M, Hatabu H, Asakura T. Parametric mapping of ex-vivo mouse lung at 9.4 Tesla with air-inflation fixation method. Proc Intl Soc Magn Reson Med 2006;14:1344.
37. Wood ML, Henkelman RM. The magnetic field dependence of the breathing artifact. Magn Reson Imaging 1986;4:387–392.
38. Bishop J, Feintuch A, Bock NA, Nieman B, Dazai J, Davidson L, Henkelman RM. Retrospective gating for mouse cardiac MRI. Magn Reson Med 2006;55:472–477.
39. Nieman BJ, Bock NA, Bishop J, Sled JG, Chen XJ, Henkelman RM. Fast spin-echo for multiple mouse magnetic resonance phenotyping. Magn Reson Med 2005;54:532–537.
40. Chen Q, Jakob PM, Griswold MA, Levin DL, Hatabu H, Edelman RR. Oxygen enhanced MR ventilation imaging of the lung. MAGMA 1998; 7:153–161.
41. Naish JH, Parker GJ, Beatty PC, Jackson A, Young SS, Waterton JC, Taylor CJ. Improved quantitative dynamic regional oxygen-enhanced pulmonary imaging using image registration. Magn Reson Med 2005; 54:464–469.
42. Bankier AA, O'Donnell CR, Mai VM, Storey P, De Maertelaer V, Edelman RR, Chen Q. Impact of lung volume on MR signal intensity changes of the lung parenchyma. J Magn Reson Imaging 2004;20:961–966.